

PromptDepthAnything++: Accurate 4K Metric Depth Estimation via Pattern-Agnostic Prompting

Haotong Lin Sida Peng Qinglin Yang Peishan Yang Jiaming Sun
Ruizhen Hu Kai Xu Hujun Bao Bingyi Kang Xiaowei Zhou†

Abstract—Prompts play a critical role in unleashing the power of language and vision foundation models for specific tasks. For the first time, we introduce prompting into depth foundation models, creating a new paradigm for metric depth estimation termed Prompt Depth Anything. Specifically, we use a low-cost LiDAR as the prompt to guide the Depth Anything model for accurate metric depth output, achieving up to 4K resolution. Our approach centers on a concise prompt fusion design that integrates the LiDAR at multiple scales within the depth decoder. To address training challenges posed by limited datasets containing both LiDAR depth and precise GT depth, we propose a scalable data pipeline that includes synthetic data LiDAR simulation and real data pseudo GT depth generation. To further extend our method to work with any prompt depth points, we propose a new prompting mechanism, which serializes the input depth points into tokens and uses self-attention to enhance image tokens from depth foundation models. Our approach sets new state-of-the-arts on 8 zero-shot depth benchmarks and benefits downstream applications, including 3D reconstruction and generalized robotic grasping. The code is available at <https://github.com/DepthAnything/PromptDA>.

estimation by treating it as a downstream task, *i.e.*, prompting a depth foundation model with metric information. We believe this prompt can take any form as long as the scale information is provided, *e.g.*, camera intrinsics. In this paper, we validate the feasibility of the paradigm by choosing low-cost LiDAR as the prompt for two reasons. First, it provides precise metric scale information. Second, it is widely available, even in common mobile devices (*e.g.*, Apple iPhone has a LiDAR).

Specifically, based on Depth Anything [2], we propose *Prompt Depth Anything*, which achieves 4K resolution accurate metric depth estimation. At the core of our method is a concise prompt fusion architecture tailored for the DPT-based [16] depth foundation models [2], [9]. The prompt fusion architecture integrates the LiDAR depth at multiple scales within the DPT decoder, fusing the LiDAR features for depth decoding. The metric prompt provides precise spatial distance information, making the depth foundation model particularly serve as a local shape learner, resulting in accurate and high-resolution metric depth estimation.

Training *Prompt Depth Anything* requires both LiDAR depth and precise GT depth. However, existing synthetic data [17] lacks LiDAR depth, and real-world data [18] with LiDAR only has an imprecise GT depth of bad edges. To solve this challenge, we propose a scalable data pipeline that simulates low-resolution, noisy LiDAR for synthetic data and generates pseudo GT depth with high-quality edges for real data using a reconstruction method [19]. To mitigate errors in the pseudo GT depth from the 3D reconstruction, we introduce an edge-aware depth loss that leverages only the gradient of pseudo GT depth, which is prominent at edges. We experimentally demonstrate that these efforts result in highly accurate depth estimation.

We evaluate the proposed method on ARKitScenes [20] and ScanNet++ [18] datasets containing iPhone ARKit depth. It consistently exhibits state-of-the-art performance across datasets and metrics. Even our zero-shot model achieves better performance compared to other methods [2], [5] in non-zero-shot testing, highlighting the generalization ability of prompting a foundation model. We also show that the foundation model and prompt of *Prompt Depth Anything* can be replaced with DepthPro [9] and vehicle LiDAR [21], respectively. Furthermore, we demonstrate that it benefits several downstream applications, including 3D reconstruction and generalized robotic object grasping.

A preliminary version of this work [22] was presented at CVPR 2025. In this extension, we first introduce a new prompting mechanism that enables foundation models to work

I. INTRODUCTION

High-quality depth perception is a fundamental challenge in computer vision and robotics. Recent monocular depth estimation has experienced a significant leap by scaling the model or data, leading to the flourishing of depth foundation models [1]–[4]. These models demonstrate strong abilities in producing high-quality relative depth, but suffer from scale ambiguity, hindering their practical applications in autonomous driving and robotic manipulation, *etc.* Therefore, significant efforts have been made to achieve metric depth estimation, by either finetuning depth foundation models [5], [6] on metric datasets or training metric depth models with image intrinsics as additional inputs [7]–[10]. However, neither of them can address the problem properly, as illustrated in Fig. 1(b).

A natural question thus arises: *Do these foundation models truly lack utility in accurate metric depth estimation?* This reminds us to closely examine the foundation models in natural language [11], [12] and vision [13]–[15], which often involve pre-training and instruction tuning stages. A properly designed *prompt* and a *instruction dataset* can unlock the power of foundation models on downstream tasks. Inspired by these successes, we propose a new paradigm for metric depth

Haotong Lin, Sida Peng, Qinglin Yang, Peishan Yang, Jiaming Sun, Hujun Bao and Xiaowei Zhou are with Zhejiang University.
Ruizhen Hu is with Shenzhen University.
Kai Xu is with National University of Defense Technology.
Bingyi Kang is with National University of Singapore.
Corresponding author†: Xiaowei Zhou.

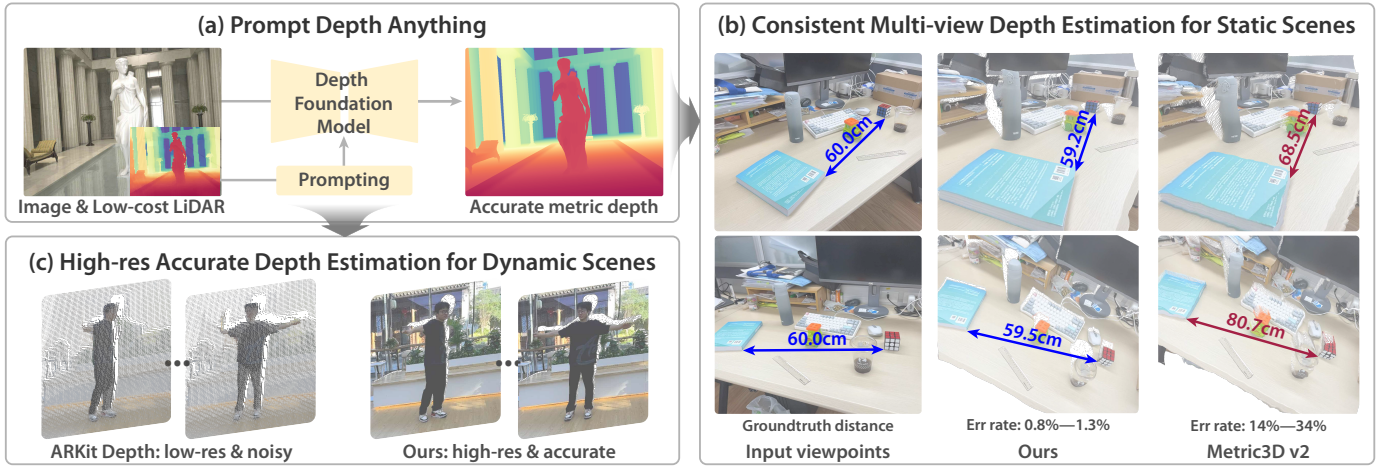


Fig. 1. **Illustration and capabilities of Prompt Depth Anything.** (a) *Prompt Depth Anything* is a new paradigm for metric depth estimation, which is formulated as prompting a depth foundation model with a metric prompt, specifically utilizing a low-cost LiDAR as the prompt. (b) Our method enables consistent depth estimation, addressing the limitations of Metric3D v2 that suffer from inaccurate scale and inconsistency. (c) It achieves accurate 4K accurate depth estimation, significantly surpassing ARKit LiDAR Depth (240×320).

with pattern-agnostic prompt depth points. Additionally, we include experiments on six more zero-shot depth benchmarks involving indoor [23]–[25], outdoor [26] and autonomous driving scenes [21], [27], further validating the effectiveness and robustness of our framework. We also compare our approach against more recent baselines involving depth completion methods [28]–[31]. Furthermore, we investigate the potential of our prompting mechanism for multi-view stereo (MVS) reconstruction by using Structure-from-Motion (SfM) points as prompts. Surprisingly, our method outperforms leading MVS methods [32], [33] by a large margin without any further fine-tuning, demonstrating the general effectiveness of our pattern-agnostic prompting approach. The code has been made publicly available at <https://github.com/DepthAnything/PromptDA>, which has garnered over 800 stars.

In summary, this work has the following contributions:

- *Prompt Depth Anything*, a new paradigm for metric depth estimation by prompting a depth foundation model with a low-cost LiDAR as the metric prompt.
- A concise prompt fusion architecture for prompting validation and a new pattern-agnostic prompting mechanism, a scalable data pipeline, and an edge-aware depth loss to train *Prompt Depth Anything*.
- State-of-the-art depth estimation performance on benchmarks for depth upsampling [18], [20] and depth completion [21], [23]–[27], showing the extensibility of replacing different depth foundation models and LiDAR sensors.
- State-of-the-art performance on MVS reconstruction by simply taking SfM points as prompting input without any further fine-tuning, showing the general effectiveness of our pattern-agnostic prompting approach.
- Highlighting benefits for several downstream applications including 3D reconstruction and robotic object grasping.

II. RELATED WORK

Monocular depth estimation. Traditional methods [34], [35] rely on hand-crafted features for depth estimation. With

the advent of deep learning, this field has seen significant advancements. Early learning-based approaches [36], [37] are often limited to a single dataset, lacking generalization capabilities. To enhance generalization, diverse datasets [38]–[45], affine-invariant loss [46], and more powerful network architectures [16] have been introduced. More recently, latent diffusion models [13], pre-trained on extensive image generation tasks, have been applied to depth estimation [3], [47], [48]. These models exhibit good generalization, estimating relative depth effectively, though they remain scale-agnostic. Pixel-Perfect Depth [49], [50] further performs diffusion generation directly in the pixel space, avoiding VAE-induced artifacts and producing flying-pixel-free depth maps. To achieve metric depth estimation, early methods either model the problem as global distribution classification [51]–[54] or fine-tune a depth model on metric depth datasets [5], [55], [56]. Recent methods [6]–[8], [10], [57] discuss the ambiguity in monocular metric depth estimation and address it by incorporating camera intrinsic parameters. More recently, Depth Anything 3 [58] unifies monocular and multi-view depth estimation with a single plain transformer and a unified depth-ray representation. InfiniDepth [59] enables arbitrary-resolution and fine-grained depth estimation via neural implicit fields. SHARP [60] further leverages sharp metric depth from Depth Pro [9] for real-time monocular view synthesis. Although recent methods [2], [3], [7]–[10], [47]–[49], [58], [59] exhibit strong generalization ability and claim to be depth foundation models [2], [4], [9], [10], [58], metric depth estimation remains a challenge as shown in Fig. 1(b). We seek to address this challenge by prompting the depth foundation models with a metric prompt, inspired by the success of prompting in vision and vision-language models [14], [15], [61].

Depth estimation with auxiliary sensors. Obtaining dense depth information through active sensors typically demands high power consumption [33], [62]–[66]. A more practical approach involves utilizing a low-power active sensor to

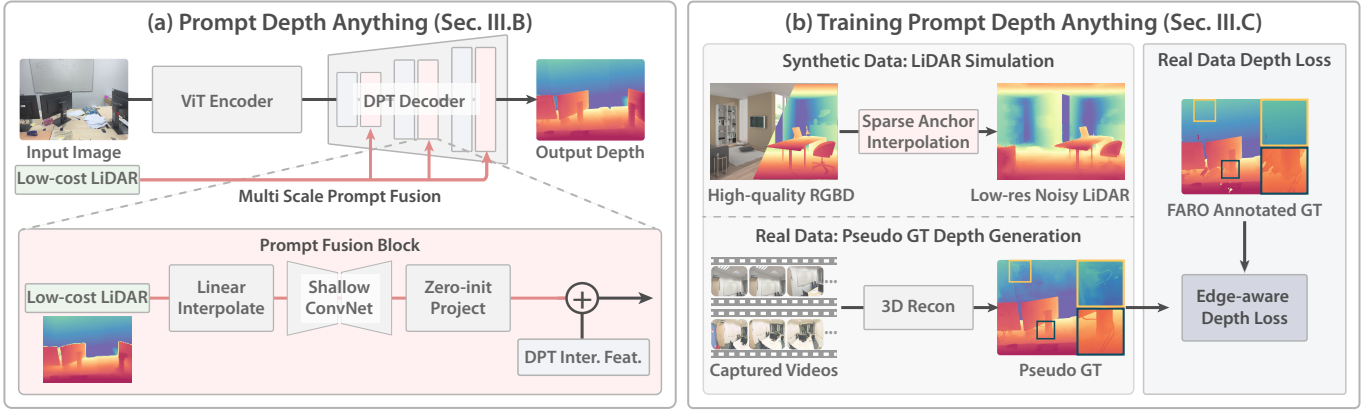


Fig. 2. **Overview of Prompt Depth Anything.** (a) *Prompt Depth Anything* builds on a depth foundation model [2] with a ViT encoder and a DPT decoder, and adds a multi-scale prompt fusion design, using a prompt fusion block to fuse the metric information at each scale. (b) Since training requires both low-cost LiDAR and precise GT depth, we propose a scalable data pipeline that simulates LiDAR depth for synthetic data with precise GT depth, and generates pseudo GT depth for real data with LiDAR. An edge-aware depth loss is proposed to merge accurate edges from pseudo GT depth with accurate depth in textureless areas from FARO annotated GT depth on real data.

capture sparse depth, which can then be completed into dense maps. Many studies investigate methods to fill in sparse depth data. Early works rely on filter-based [67]–[69] and optimization-based [70], [71] techniques for depth completion. More recent studies [28], [32], [65], [72]–[80] adopt learning-based approaches for depth completion. Among them, LingBot-Depth [80] employs masked depth modeling with vision transformers to refine sparse and noisy depth sensor data for robotics applications. Typically, these methods are not tested on real indoor LiDAR data but rather on simulated sparse lidar for depth datasets such as NYUv2 [36] to reconstruct complete depth. This is because real testing setups require both low-power and high-power LiDAR sensors. More recent works have collected both low-power and high-power LiDAR data. To collect such data, DELTA [81] builds a suite to collect data using L5 and Intel RealSense 435i, while three other datasets [18], [20], [82] are collected using iPhone LiDAR and FARO LiDAR. We focus on the latter, as iPhone is widely available. A recent work similar to ours is Depth Prompting [83]. Our approach differs in that we use a network to take sparse depth as a prompt for the depth foundation model, achieving specific output. In contrast, they fuse sparse depth with features from the depth foundation model to post-process the foundation model output, which does not constitute prompting a foundation model.

III. METHOD

Monocular depth estimation models [1], [2], [9] are becoming depth foundation models from large-scale data training. However, due to the inherent ambiguities, they cannot achieve high accuracy on metric depth estimation as shown in Fig. 1(b). Inspired by the success of prompting for vision [13], [14], [84] and language [12] foundation models, we propose *Prompt Depth Anything* prompting the depth foundation model with a metric prompt to achieve metric depth estimation. We take the low-cost LiDAR as the metric prompt in this work, as it has recently been integrated into lots of smartphones, making this setup highly practical. To be specific, we aim to prompt

the depth foundation model to unleash its power for accurate metric depth estimation.

A. Preliminary: Depth Foundation Model

Current depth foundation models [1], [2], [8], [85] generally share similar network structures of DPT [16] networks. Specifically, given an image $\mathbf{I} \in \mathbb{R}^{C \times H \times W}$, they take a vision transformer (ViT) with multiple stages to extract tokenized image features $\{\mathbf{T}_i\}$, where $\mathbf{T}_i \in \mathbb{R}^{C_i \times (\frac{H}{p} \times \frac{W}{p} + 1)}$ represents the feature map at stage S_i , D_i is the feature dimension at stage S_i , and p is the patch size. The DPT decoder reassembles features from different stages into image-like representations $\mathbf{F}_i \in \mathbb{R}^{D_i \times \frac{H}{p} \times \frac{W}{p}}$ with the reassemble operation [16]. Finally, a sequence of convolutional blending steps are applied to merge features \mathbf{F}_i across different stages, predicting a dense depth map $\mathbf{D} \in \mathbb{R}^{H \times W}$. We note that there exists another line of depth foundation models [3], [4], [47] that use the image diffusion model [86] to estimate depth maps. Due to the high computational cost of diffusion models, we only consider DPT-based depth foundation models [2], [9] as our base model for real-time performance in this work.

B. Prompt Depth Anything

In this section, we seek to find a concise way to incorporate a low-cost LiDAR (i.e., a low-resolution and noisy depth map) as a prompt into the depth foundation model. To this end, we propose a concise prompt fusion architecture tailored for the DPT-based [16] depth foundation models to integrate low-resolution depth information. As shown in Fig. 2(a), the prompt fusion architecture integrates low-resolution depth information at multiple scales within the DPT Decoder. Specifically, for each scale S_i in the DPT Decoder, a low-resolution depth map $\mathbf{L} \in \mathbb{R}^{1 \times H_L \times W_L}$ is firstly bilinearly resized to match the spatial dimensions of the current scale $\mathbb{R}^{1 \times H_i \times W_i}$. Then, the resized depth map is passed through a shallow convolutional network to extract depth features. After that, the extracted features are projected to the same dimension as the image features



Fig. 3. Effects on the synthetic data lidar simulation and real data pseudo GT generation with the edge-aware depth loss. The middle and right columns are the depth prediction results of our different models. The two rows highlight the significance of sparse anchor interpolation for lidar simulation and pseudo GT generation with edge-aware depth loss, respectively.

$\mathbf{F}_i \in \mathbb{R}^{C_i \times H_i \times W_i}$ using a zero-initialized convolutional layer. Finally, the depth features are added to the DPT intermediate features for depth decoding. The illustration of this block design is shown in Fig. 2.

The proposed design has the following advantages. Firstly, it introduces only 5.7% additional computational overhead (1.789 TFLOPs v.s. 1.691 TFLOPs for a 756×1008 image) to the original depth foundation model, and effectively addresses the ambiguity issue inherent in the depth foundation model as demonstrated in Tab. VI(b). Secondly, it fully inherits the capabilities of the depth foundation model because its encoder and decoder are initialized from the foundation model [2], and the proposed fusion architecture is zero-initialized, ensuring that the initial output is identical to that of the foundation model. We experimentally verify the importance of inheriting from a pretrained depth foundation model as shown in Tab. VI(c).

Optional designs. Inspired by conditional image generation methods [61], [87], [88], we also explore various potential prompt conditioning designs into the depth foundation model. Specifically, we experimented with the following designs: a) Adaptive LayerNorm [88], [89] which adapts the layer normalization parameters of the encoder blocks based on the conditioning input, b) CrossAttention [90] which injects a cross attention block after each self-attention block and integrates the conditioning input through cross-attention mechanisms, and c) ControlNet [61] which copies the encoder blocks and inputs control signals to the copied blocks to control the output depth. As shown in Tab. VI(d,e,f), our experiments reveal that these designs do not perform as well as the proposed fusion block. A plausible reason is that they are designed to integrate cross-modal information (e.g., text prompts), which does not effectively utilize the pixel alignment characteristics between the input low-res LiDAR and the output depth. We detail these optional designs in the supp.

C. Training Prompt Depth Anything

Training *Prompt Depth Anything* simultaneously requires a low-cost LiDAR and precise GT depth. However, synthetic

data [17] do not contain LiDAR depth, real-world data with noisy LiDAR depth [18] only have imprecise depth annotations. Therefore, we propose a LiDAR simulation method for synthetic data and generate pseudo GT depth from ZipNeRF [19] with an edge-aware depth loss for real data. Note that more effective approaches [91], [92] can be applied.

Synthetic data: LiDAR simulation. A LiDAR depth map is low-resolution and noisy. The naive approach for simulating it is to directly downsample the synthetic data depth map. However, this method leads to the model learning depth super-resolution, as shown in Fig. 3, meaning that the model does not correct the LiDAR noise. To simulate the noise, we introduce a sparse anchor interpolation method. Specifically, we first downsample the GT depth map to low-resolution (192×256 , exactly the depth resolution of iPhone ARKit Depth). Then we sample points on this depth map using a distorted grid with a stride (7 in practice). The remaining depth values are interpolated from these points using RGB similarity with KNN. As shown in Fig. 3, it effectively simulates LiDAR noise and results in better depth prediction. We provide visualization results of the simulated LiDAR in the supp.

Real Data: Pseudo GT depth generation. We also add real data [18] to our training data. The annotated depth in ScanNet++ [18] is re-rendered from a mesh scanned by a high-power LiDAR sensor (FARO Focus Premium laser scanner). Due to the presence of many occlusions in the scene, several scan positions (typically 4 in a medium-sized scene in ScanNet++) result in an incomplete scanned mesh, leading to depth maps with numerous holes and poor edge quality, as illustrated in Fig. 2(b). Motivated by the success of reconstruction methods [19], [93], we propose using ZipNeRF [19] to recover high-quality depth maps. Specifically, we train Zip-NeRF for each scene in ScanNet++ and re-rendered pseudo GT depth. To provide Zip-NeRF with high-quality and dense observations, we detect unblurred frames in Scannet++iPhone videos, and additionally utilize DSLR videos to provide high-quality dense-view images.

Real Data: Edge-aware depth loss. Although Zip-NeRF can generate high-quality edge depth, reconstructing textureless and reflective regions remains challenging as shown in Fig. 2(b). In contrast, these areas (e.g., walls, floors, and ceilings etc.) are usually planar with few occlusions, and the annotations depth in FARO rendered depth is good in these regions. This motivates us to leverage the strengths of both. We propose an edge-aware depth loss to meet these requirements. Specifically, we use the FARO scanned mesh depth and the gradient of the pseudo GT depth to supervise output depth and the gradient of the output depth, respectively:

$$\mathcal{L}_{\text{edge}} = L_1(\mathbf{D}_{\text{gt}}, \hat{\mathbf{D}}) + \lambda \cdot \mathcal{L}_{\text{grad}}(\mathbf{D}_{\text{pseudo}}, \hat{\mathbf{D}}), \quad (1)$$

$$\mathcal{L}_{\text{grad}}(\mathbf{D}_{\text{pseudo}}, \hat{\mathbf{D}}) = (|\frac{\partial(\hat{\mathbf{D}} - \mathbf{D}_{\text{pseudo}})}{\partial x}| + |\frac{\partial(\hat{\mathbf{D}} - \mathbf{D}_{\text{pseudo}})}{\partial y}|). \quad (2)$$

In practice, we set $\lambda = 0.5$. The depth gradient is mainly prominent at the edges, which is exactly where the pseudo GT depth excels. The gradient loss encourages the model to learn the accurate edges from the pseudo GT depth, while the L1 loss encourages the model to learn the overall depth, ultimately

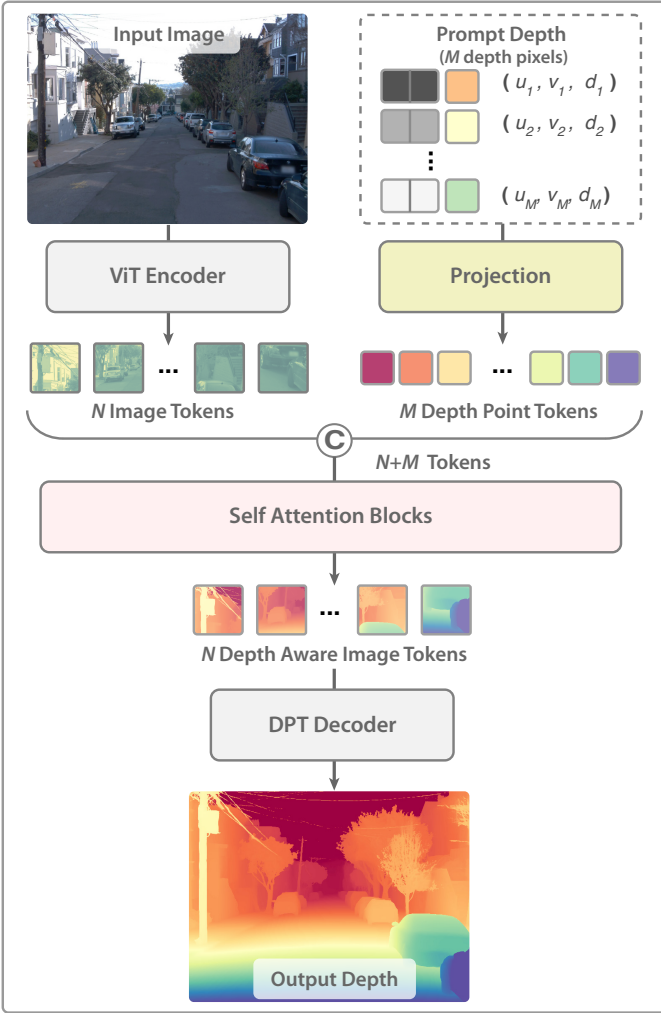


Fig. 4. **Pipeline of pattern-agnostic depth prompting.** To improve the robustness of *Prompt Depth Anything* against prompt depth map patterns, we propose converting prompt depth points into a sequence of tokens, thereby mitigating pattern-specific influences. We first employ an MLP to project the prompt depth points into a sequence of tokens. The resulting prompt tokens are then concatenated with the image tokens and processed through a series of self-attention layers incorporating 2D uv position encoding. After that, the image tokens are enhanced by the prompt depth points, and the enhanced image tokens are fed into a DPT Decoder to reconstruct the depth map. The depth tokens output by the self-attention layers are simply discarded.

leading to excellent depth prediction. We experimentally verify the effectiveness of the edge-aware depth loss in Tab. VI(j) and Fig. 3.

D. Pattern Agnostic Depth Prompting

In the previous section, we presented a systematic framework for prompting depth foundation models and practical training data construction methods. This design particularly excels at handling low-resolution prompt depth, typically for depth upsampling [18], [20], but does not address various specific prompt characteristics, such as the diverse patterns of sensors in the real world. For instance, Intel RealSense sensors exhibit different patterns: they may have random holes due to occlusion between the depth sensor and RGB sensor, or due to objects being too far away, or from scanning reflective surfaces.

Without specific prompting design, previous models would produce unsatisfactory results when encountering prompt depth of extreme random patterns.

To address the challenge of diverse patterns for prompt depth in practical applications, we propose a new prompting mechanism that can accept pattern-agnostic sparse points as prompts, thereby broadening the applicability of our method. Previous methods typically design complex convolutional networks or vision transformers to extract features from sparse depth *maps* and then fuse this information with the image branch to output depth maps. Instead of using *map*-based fusion, we propose a novel fusion module that serializes the sparse depth map into a *sequence* of tokens for network processing. Since the network no longer needs to learn the characteristics of sparse maps (such as random holes that are unfriendly to network learning), but instead learns from serialized tokens, we can robustly handle various different point patterns.

Specifically, given a sparse depth map, we first serialize the valid depth pixels into a sequence of points (u, v, d) , where u and v are the pixel coordinates and d is the depth value. Then, an MLP is used to project the depth point into a token with the same dimension as the image token. Then, the resulting depth tokens are concatenated with the image tokens extracted from the depth foundation model and passed through a series of self-attention layers. To connect the depth tokens with the image tokens, we use 2D UV encoding to encode the position of image and depth point tokens, and the encoding is added to the query and key components of the self-attention layers. After processing through the self-attention layers, the image tokens are enhanced by the depth information, while the depth tokens are discarded as they serve only as auxiliary information for enhancing the image features. The enhanced image tokens are also processed with a zero-init. MLP and then plus the original image tokens to get the final image tokens, which ensuring inheriting the foundation model ability. The final image tokens are then fed into the DPT Decoder to reconstruct the final depth map. This design enables our model to handle various sensor patterns robustly, as it learns to extract meaningful depth information from tokenized representations rather than being constrained by specific spatial patterns.

E. Implementation Details

In this section, we provide essential information about the network design, depth normalization, and training details. Please refer to the supp. for more details.

Network details. We utilize the ViT-large model as our backbone model. The shallow convolutional network comprises two convolutional layers with a kernel size of 3 and a stride of 1, using ReLU as the non-linear activation function. The zero-init project layer is a 1×1 convolution layer.

Depth normalization. The irregular range of input depth data can hinder network convergence. To address this, we normalize the LiDAR data using linear scaling to the range $[0, 1]$, based on its minimum and maximum values. The network output is also normalized with the same scaling factor from LiDAR data, ensuring consistent scales and facilitating easier convergence during training. For pattern-agnostic prompting, as the prompt

TABLE I
 QUANTITATIVE COMPARISONS ON SCANNET++ DATASET. THE TERMS **NET.**, **POST.** AND **W/O LiDAR** REFER TO THE LiDAR DEPTH USAGE OF MODELS. METHODS MARKED WITH * ARE FINETUNED WITH THEIR RELEASED CODE ON ARKITSCENES [20] AND SCANNET++ [18] DATASETS.

Zero Shot	Net. / Post. / w/o LiDAR	Depth Estimation				TSDF Reconstruction				
		L1 ↓	RMSE ↓	AbsRel ↓	$\delta_{0.5}$ ↑	Acc ↓	Comp ↓	Prec ↑	Recall ↑	F-score ↑
No	Ours	0.0250	0.0829	0.0175	0.9781	0.0699	0.0616	0.7255	0.8187	0.7619
	MSPF*	0.0326	0.0975	0.0226	0.9674	0.0772	0.0695	0.6738	0.7761	0.7133
	DepthAny. v2*	0.0510	0.1010	0.0371	0.9437	0.0808	0.0735	0.6275	0.7107	0.6595
	ZoeDepth*	0.0582	0.1069	0.0416	0.9325	0.0881	0.0801	0.5721	0.6640	0.6083
	DepthAny. v2*	0.0903	0.1347	0.0624	0.8657	0.1264	0.0917	0.4256	0.5954	0.4882
	ZoeDepth*	0.1675	0.1984	0.1278	0.5807	0.1567	0.1553	0.2164	0.2553	0.2323
Yes	Ours_{syn}	0.0327	0.0966	0.0224	0.9700	0.0746	0.0666	0.6903	0.7931	0.7307
	D.P.	0.0353	0.0983	0.0242	0.9657	0.0820	0.0747	0.6431	0.7234	0.6734
	ARKit Depth	0.0351	0.0987	0.0241	0.9659	0.0811	0.0743	0.6484	0.7280	0.6785
	DepthAny. v2	0.0592	0.1145	0.0402	0.9404	0.0881	0.0747	0.5562	0.6946	0.6127
	Depth Pro	0.0638	0.1212	0.0510	0.9212	0.0904	0.0760	0.5695	0.6916	0.6187
	Metric3D v2	0.0585	0.3087	0.0419	0.9529	0.0785	0.0752	0.6216	0.6994	0.6515
	Marigold	0.0828	0.1412	0.0603	0.8718	0.0999	0.0781	0.5128	0.6694	0.5740
	DepthPro	0.2406	0.2836	0.2015	0.5216	0.1537	0.1467	0.2684	0.3752	0.3086
	Metric3D v2	0.1226	0.3403	0.0841	0.8009	0.0881	0.0801	0.5721	0.6640	0.6083

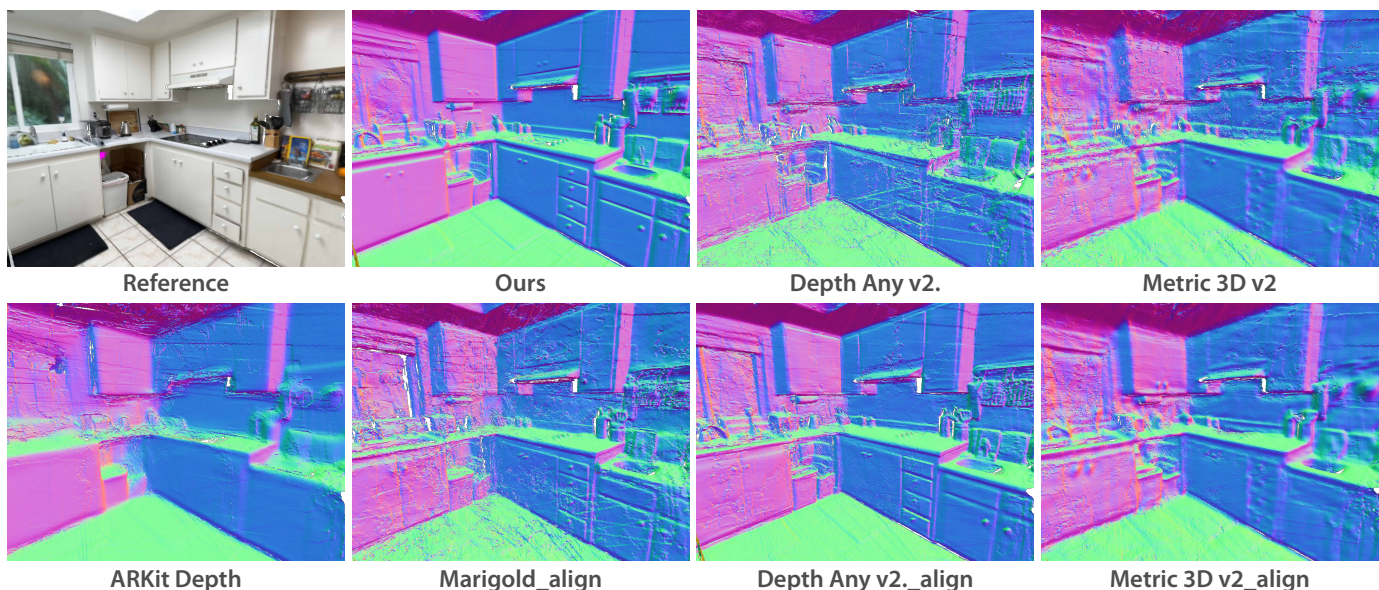


Fig. 5. **Qualitative comparisons of TSDF reconstruction.** *_align denotes the scale-shift corrected depth with ARKit depth.

depth points are generally incomplete, the near far range of the prompt depth may not match the near far range of the image depth. In practical, we use the median value of prompt depth points to normalize the prompt depth and make the model output the corresponding normalized depth.

Training details. We initiate training from the metric model released by Depth Anything v2 [2], incorporating a 10K step warm-up phase. During this warm-up phase, we fine-tune this metric model to output a normalized depth derived from the linear scaling of LiDAR data. Subsequently, we train our model for 200K steps. During the training process, the batch size is set to 2, utilizing 8 GPUs. We employ the AdamW optimizer, with a learning rate of 5e-6 for the ViT backbone and 5e-5 for the other parameters.

IV. EXPERIMENTS

A. Experimental Setup

Prompting a depth foundation model with depth priors can be categorized into two types of tasks: depth upsampling and depth completion. For depth prompting with upsampling task, we mainly conduct experiments on the HyperSim synthetic dataset [17] and two real-world datasets: ScanNet++ [18] and ARKitScenes [20], which provide iPhone RGB-LiDAR data (192×256 resolution) and annotated depth from a high-power LiDAR (1440×1920 resolution). We follow the suggested training and evaluation protocol in [20] for ARKitScenes, where 40K images are used for training and 5K images for evaluation. For the ScanNet++ dataset, we randomly select 20 scenes from its 50 validation scenes, amounting to approximately 5K images for our validation and the training set are from its 230 training scenes, containing about 60K images. To ensure a fair comparison, we additionally train a

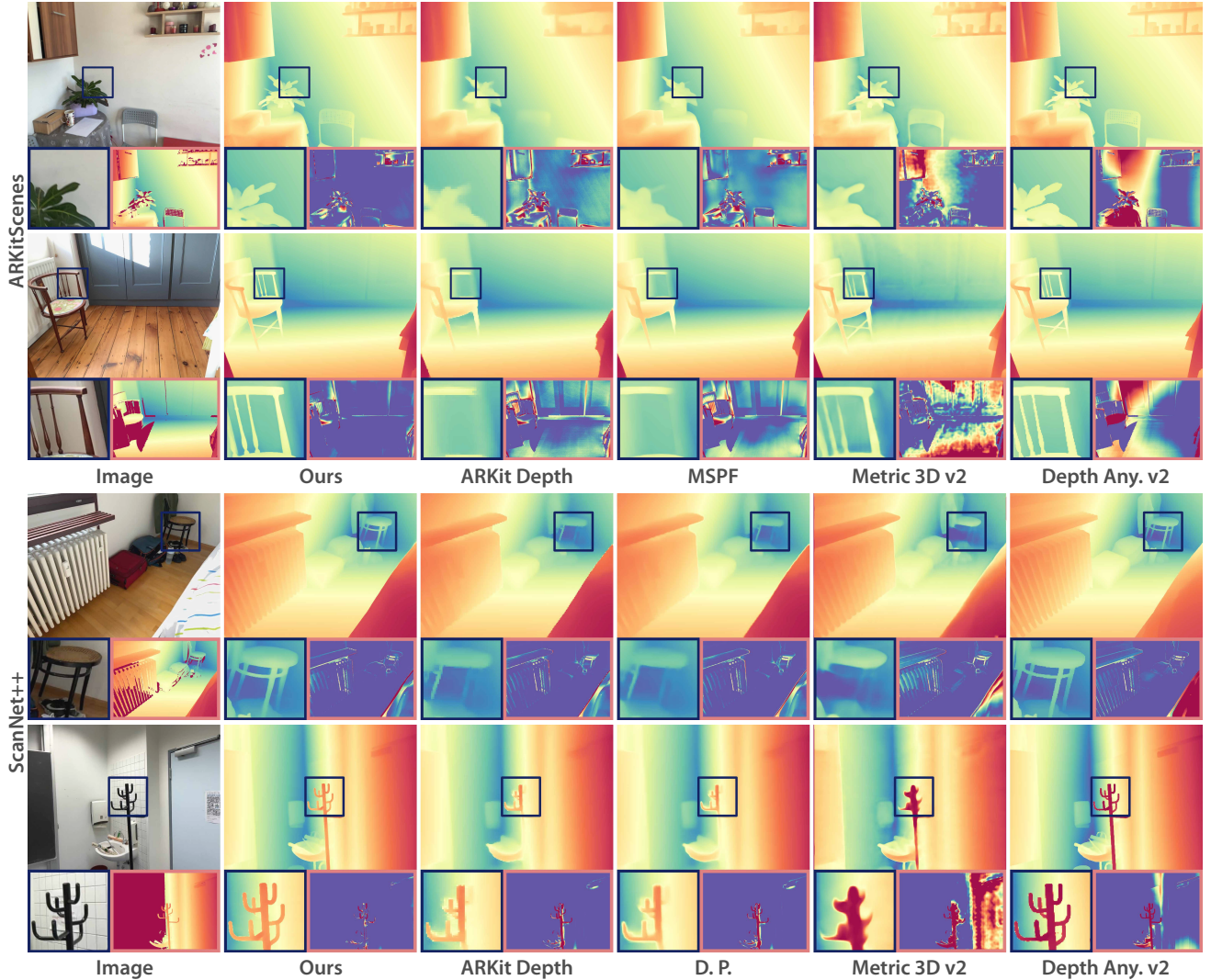


Fig. 6. **Qualitative comparisons with the state-of-the-art.** “Metric3D v2” and “Depth Any. v2” are scale-shift corrected with ARKit depth. The pink boxes denote the GT depth and depth percentage error map, where red represents high error, and blue indicates low error.

TABLE II

COMPARISONS ON ARKITSCENES DATASET. THE TERMS NET. , POST. AND W/O LiDAR REFER TO THE LiDAR DEPTH USAGE OF MODELS, WHERE “NET.” DENOTES NETWORK FUSION, “POST.” INDICATES POST-ALIGNMENT, AND “W/O LiDAR” MEANS METRIC DEPTH.

Zero Shot	Net. / Post. / w/o LiDAR	384 × 512		768x1024		1440x1920	
		L1 ↓	RMSE ↓	L1 ↓	RMSE ↓	L1 ↓	RMSE ↓
No	Ours	0.0135	0.0326	0.0132	0.0315	0.0138	0.0316
	MSPF	0.0153	0.0369	0.0149	0.0362	0.0152	0.0363
	Depth Pro*	0.0437	0.0672	0.0435	0.0665	0.0425	0.0654
	DepthAny. v2*	0.0464	0.0715	0.0423	0.0660	0.0497	0.0764
	ZoeDepth*	0.0831	0.2873	0.0679	0.1421	0.0529	0.0793
	Depth Pro*	0.1222	0.1424	0.1225	0.1427	0.1244	0.1444
Yes	DepthAny. v2*	0.0978	0.1180	0.0771	0.0647	0.0906	0.1125
	ZoeDepth*	0.2101	0.2784	0.1780	0.2319	0.1566	0.1788
	Ours_{syn}	0.0161	0.0376	0.0163	0.0371	0.0170	0.0376
	D.P.	0.0251	0.0422	0.0253	0.0422	0.0249	0.0422
	BPNet	0.1494	0.2106	0.1493	0.2107	0.1491	0.2100
	ARKit Depth	0.0251	0.0424	0.0250	0.0423	0.0254	0.0426
	DepthAny. v2	0.0716	0.1686	0.0616	0.1368	0.0494	0.0764
	Metric3D v2	0.0626	0.2104	0.0524	0.1721	0.0402	0.1045
	ZoeDepth	0.1007	0.1917	0.0890	0.1627	0.0762	0.1135
	Lotus	0.0624	0.0970	0.0621	0.0962	0.0622	0.0965
	Marigold	0.0908	0.1849	0.0807	0.1565	0.0692	0.1065
	Metric3D v2	0.1777	0.2766	0.1663	0.2491	0.1615	0.2131
ZoeDepth	0.6158	0.9577	0.5688	0.6129	0.5316	0.5605	

model with HyperSim training set to achieve zero-shot testing on ScanNet++ and ARKitScenes datasets.

For depth prompting with completion task, we train our model using common synthetic monocular depth datasets including HyperSim [17], VKITTI2 [94], TartanAir [24], UrbanSyn [95], DynamicReplica [96], datasets. We evaluate our method on a diverse set of six zero-shot datasets: three indoor scene datasets, NYUv2 [23], ScanNet [24], and DIODE [25]; one outdoor scene dataset, ETH3D [26]; and two autonomous driving datasets, KITTI [27] and Waymo [21]. All the datasets are zero-shot for our method. Prompt depth maps, serving as input, were generated by randomly selecting 1,500 points from the sensor-acquired depth maps of each dataset. We report depth accuracy metrics including AbsRel and L1 error, which stand for relative percentage error and mean absolute error in distance, respectively.

B. Comparisons with the State of the Art

For depth upsampling, we compare our method against the current SOTA depth estimation methods from two

TABLE III
 QUANTITATIVE COMPARISONS FOR DEPTH PROMPTING WITH COMPLETION TASK ON 6 ZERO-SHOT TESTING BENCHMARKS. ALL METHODS ARE RE-EVALUATED ON THE IDENTICAL TEST SET AND EXECUTED ON THE SAME MACHINE FOR A FAIR COMPARISON OF BOTH RUNTIME AND PERFORMANCE.

	FPS	NYU		Scannet		DIODE		KITTI		Waymo		ETH3D	
		AbsRel ↓	MAE ↓	AbsRel ↓	MAE ↓	AbsRel ↓	MAE ↓	AbsRel ↓	MAE ↓	AbsRel ↓	MAE ↓	AbsRel ↓	MAE ↓
BP-Net	23.81	3.221	0.100	2.678	0.052	3.947	0.251	7.769	1.601	6.203	1.556	5.004	0.478
Marigold-DC	0.05	1.250	0.036	1.190	0.022	0.866	0.030	2.894	0.556	2.875	0.693	1.050	0.066
Omni-DC	7.77	2.164	0.061	2.237	0.042	1.120	0.051	5.670	1.065	7.805	1.864	3.350	0.219
PriorDepthAny.	28.57	1.218	0.036	1.283	0.023	0.471	0.019	2.442	0.573	3.225	0.931	0.791	0.058
Ours	42.02	0.890	0.027	0.900	0.017	0.255	0.011	2.130	0.481	2.900	0.791	1.040	0.054

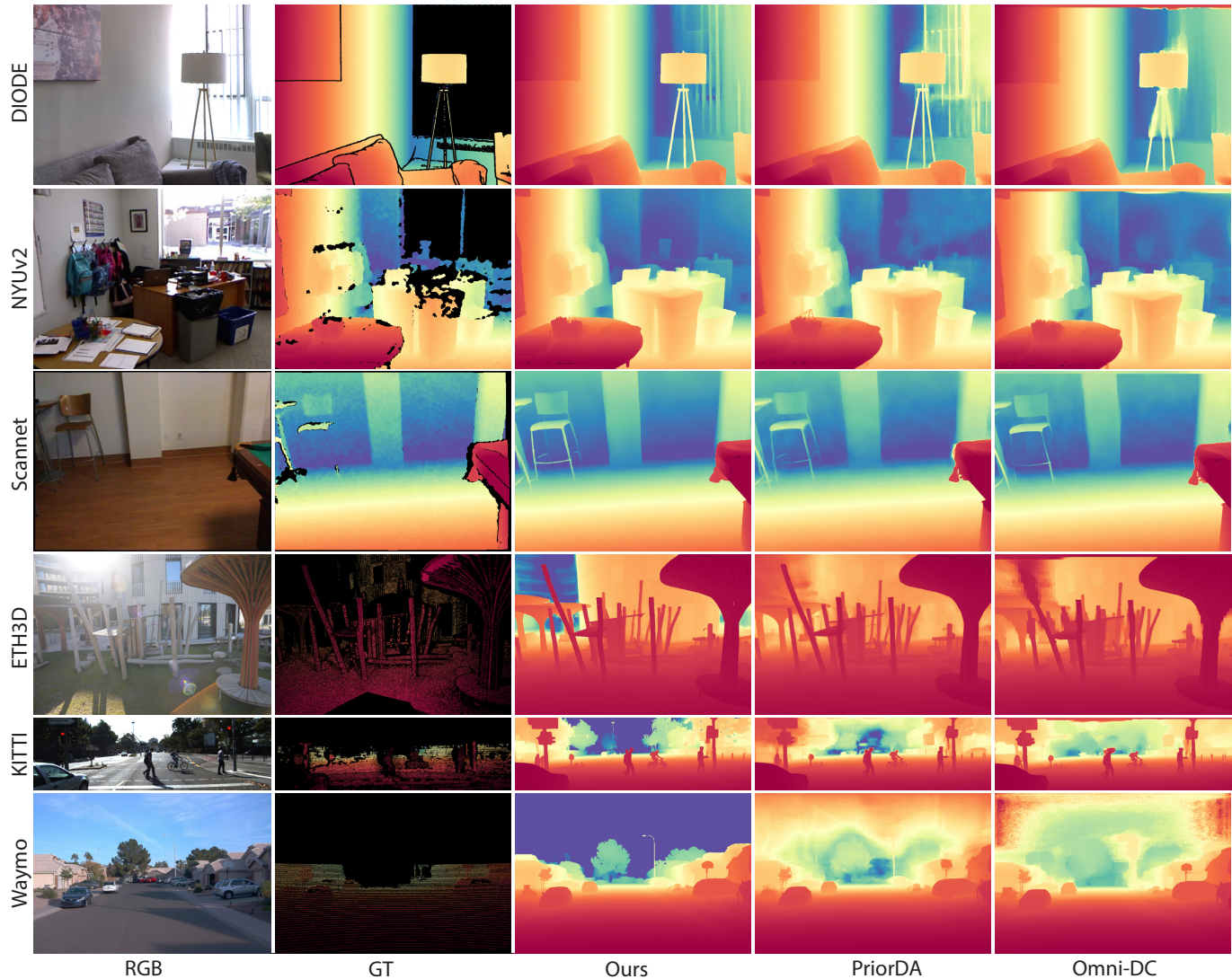


Fig. 7. Qualitative comparisons with SOTA depth completion methods. All the depth maps are normalizing with the same parameters for visualizing.

classes: *Monocular depth estimation (MDE)* and *depth completion/upsampling*. For MDE methods, we compare our method with Metric3D v2 [10], ZoeDepth [5], DepthPro [9], Depth Anything v1 and v2 [1], [2] (short for DepthAny. v1 and v2), Marigold [3] and Lotus [47]. For depth completion/upsampling methods, we compare our method with BPNet [28], Depth Prompting [83] (short for D.P.), MSPF [97]. To make a fair comparison with MDE methods, we align their predictions with ARKit LiDAR depth using the RANSAC align method. According to whether they have seen the testing data types during training, we divide methods into two categories: *zero-*

shot and *non zero-shot*. We train a model $Ours_{syn}$ only with HyperSim training set to make comparisons with the zero-shot methods. As shown in Tabs. I and II and Fig. 6, our method consistently outperforms the existing methods. Note that $Ours_{syn}$ achieves better performance than all non-zero-shot models [2], [97] on ScanNet++, highlighting the generalization ability of prompting a depth foundation model. We also evaluate different models on ScanNet++ using 3D reconstruction metrics, which reflects the 3D consistency of depth estimation results. Fig. 5 visualize normal maps of 3D reconstruction results for different methods. As shown in Tab. I and Fig. 5, our method

TABLE IV
 QUANTITATIVE RESULTS ON DTU DATASET. WE EVALUATE CHAMFER DISTANCE OF EACH METHOD ON EACH SCENE (MEASURED IN MILLIMETERS) AND HIGHLIGHT THE BEST, SECOND-BEST, AND THIRD-BEST PERFORMING METRICS IN THE TABLE.

	COLMAP	RealityCapture	VoISDF	MonoSDF	Marigold	DepthAny.	DepthAny.v2	Metric3D	MVSNet	IGEV-MVS	DUST3R	Murre	Ours
scan24	4.45	4.19	5.24	3.47	4.77	2.99	4.07	5.99	3.16	4.20	2.24	1.31	0.82
scan37	4.67	3.85	5.09	3.61	7.61	3.77	4.33	5.26	4.36	5.05	3.43	3.14	2.52
scan40	2.51	2.26	3.99	2.10	5.34	3.01	2.54	4.13	2.59	3.47	2.77	1.53	1.00
scan55	1.90	2.49	1.42	1.05	4.75	2.10	4.07	4.22	2.35	2.79	2.40	0.92	0.61
scan63	2.81	3.49	5.10	2.37	4.07	2.98	3.05	3.14	1.88	3.05	3.71	1.19	1.11
scan65	2.92	3.97	4.33	1.38	4.15	4.10	3.61	5.00	3.28	3.16	3.22	1.98	1.16
scan69	2.12	1.91	5.36	1.41	7.38	2.73	3.16	4.20	2.32	3.16	2.49	1.25	0.84
scan83	2.05	2.49	3.15	1.85	6.00	2.38	3.29	4.78	1.88	3.17	3.34	2.16	1.39
scan97	2.93	2.37	5.78	1.74	5.38	4.17	4.86	4.54	1.87	3.62	2.71	1.40	1.19
scan105	2.05	2.27	2.07	1.10	5.26	3.45	2.79	4.85	2.06	4.16	2.84	1.07	0.75
scan106	2.01	2.90	2.79	1.46	5.36	4.40	5.24	5.44	2.25	3.09	2.69	1.26	0.91
scan110	N/A	4.60	5.73	2.28	5.51	1.97	5.29	4.69	1.92	5.97	3.08	0.95	1.01
scan114	1.10	1.38	1.20	1.25	4.65	2.53	2.41	7.82	1.40	2.49	2.20	0.82	0.47
scan118	2.72	2.57	5.64	1.44	5.63	2.94	3.01	4.36	2.43	3.23	2.52	1.18	0.70
scan122	1.64	1.76	6.20	1.45	5.99	2.88	3.57	6.78	1.94	1.90	2.51	1.07	0.78
Average	2.56	2.84	4.21	1.86	5.46	3.09	3.69	5.01	2.38	3.50	2.81	1.42	1.02

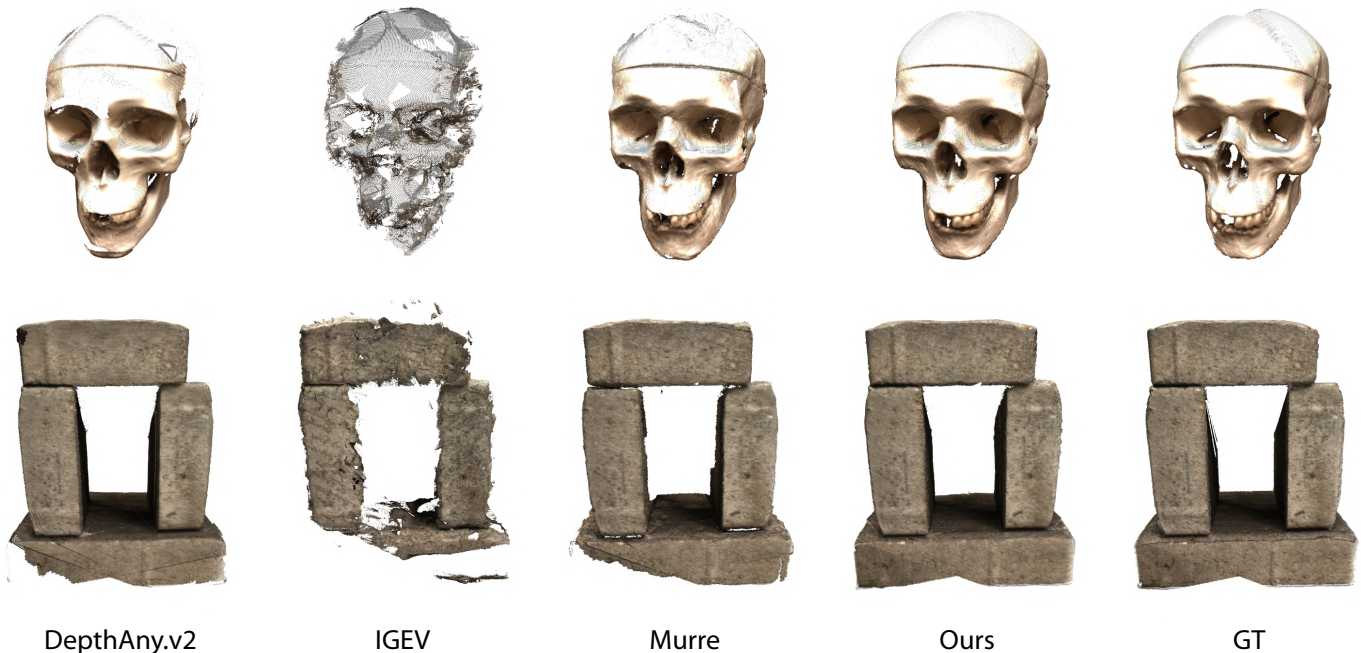


Fig. 8. Qualitative results on DTU dataset. All the methods use the same 3 input views.

TABLE V
 QUANTITATIVE RESULTS ON REPLICA DATASET. WE EVALUATE F-SCORE OF EACH METHOD ON EACH SCENE AND HIGHLIGHT THE BEST, SECOND-BEST, AND THIRD-BEST PERFORMING METRICS IN THE TABLE.

	room_1	office_0	office_2	Average
MonoSDF	-	-	-	0.86
Marigold	0.61	0.52	0.58	0.57
SparseDC	0.25	0.29	0.23	0.25
MVSNet	0.54	0.73	0.56	0.61
IGEV-MVS	0.84	0.85	0.78	0.82
Murre	0.84	0.90	0.82	0.85
Ours	0.91	0.92	0.86	0.90

presents better results than all baselines, demonstrating the superior consistency of our depth estimation results.

For the depth completion task, we compare our method with four state-of-the-art depth completion approaches [28]–[31] across six widely used benchmarks [21], [23]–[27]. [28], [30], [31] use network fusion and [29] proposes a test time optimization. These datasets are captured with different types of sensors and exhibit extremely diverse patterns, as shown in Fig. 7. Tab. III and Fig. 7 demonstrates that our method outperforms previous state-of-the-art methods in both accuracy and inference speed, making it a highly promising solution for practical applications. Note that our method even presents better results than Marigold-DC [29] which requires a long optimization process for each inference. All the benchmarks are zero-shot for our method, demonstrating the strong generalization ability of our approach across diverse

TABLE VI
QUANTITATIVE ABLATIONS ON ARKITSCENES AND SCANNET++ DATASETS. PLEASE REFER TO SEC. IV-C FOR DETAILED DESCRIPTIONS.

	ARKitScenes		ScanNet++		
	L1 ↓	AbsRel ↓	Acc ↓	Comp ↓	F-Score ↑
(a) Ours _{syn} (synthetic data)	0.0163	0.0142	0.0746	0.0666	0.7307
(b) w/o prompting	0.0605	0.0505	0.0923	0.0801	0.5696
(c) w/o foundation model	0.0194	0.0169	0.0774	0.0713	0.7077
(d) AdaLN prompting	0.0197	0.0165	0.0795	0.0725	0.6943
(e) Cross-atten. prompting	0.0523	0.0443	0.0932	0.0819	0.5595
(f) Controlnet prompting	0.0239	0.0206	0.0785	0.0726	0.6899
(g) a + ARKitScenes data	0.0134	0.0115	0.0744	0.0662	0.7341
(h) g + ScanNet++ anno. GT	0.0132	0.0114	0.0670	0.0614	0.7647
(i) g + ScanNet++ pseudo GT	0.0139	0.0121	0.0835	0.0766	0.6505
(j) Ours (h,i+edge loss)	0.0132	0.0115	0.0699	0.0616	0.7619
(k) Depth Pro as foundation	0.0169	0.0150	0.0754	0.0676	0.7202
(l) Depth Pro	0.1225	0.1038	0.0904	0.0760	0.6187

TABLE VII
QUANTITATIVE ABLATIONS FOR PROMPTING STRATEGIES. THE UPSAMPLING PROMPT INPUT IS 30×40 LOW-RES DEPTH AND COMPLETION PROMPT INPUT IS 1200 RANDOM POINTS.

	Upsampling Setting		Completion Setting	
	AbsRel ↓	MAE ↓	AbsRel ↓	MAE ↓
Upsampling Prompting Strategy	0.89	0.109	1.67	0.151
Pattern-agnostic Prompting Strategy	1.09	0.125	1.09	0.124

scenarios and sensor patterns.

3D reconstruction is an important downstream task for depth estimation. A recent trend is to use SfM depth as a condition for monocular depth models [32], combining the 3D consistency of SfM points with the strong prior of monocular depth estimation. Our pattern-agnostic prompting is highly suitable for this setting. To further demonstrate the effectiveness of our pattern-agnostic prompting, we follow the experimental setup of Murre [32], using SfM depth to prompt our model. Specifically, we evaluate our model on the DTU [98] and Replica [99] datasets. We use Detector-free SfM [100] to obtain the SfM depth for both datasets. These sparse depth maps are fed into our method to obtain dense depth predictions. We then run TSDF to obtain the final mesh results. All the evaluation settings are aligned with Murre [32] to make fair comparisons. As shown in Tabs. IV and V and Fig. 8, our method presents clear improvements over baselines. Note that our method is never finetuned on Structure-from-Motion datasets or DTU MVS datasets [98], while previous methods [32], [33] train their model on SfM or DTU MVS datasets, respectively. These comparisons highlight the effectiveness of our pattern-agnostic prompting, providing a new scalable solution for 3D reconstruction field which only needs monocular depth training.

C. Ablations and Analysis

Prompting a depth foundation model. We ablate the importance of prompting a depth foundation model with two experiments: 1) Removing the prompting. Tab. VI(b) shows a significant performance drop. 2) Removing the foundation

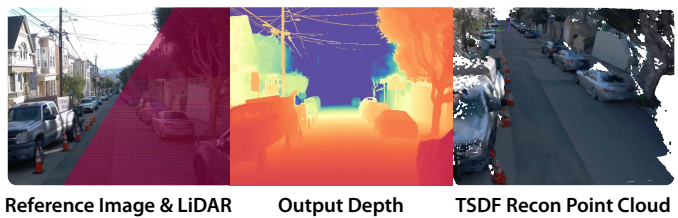


Fig. 9. Outdoor reconstruction by taking the vehicle LiDAR as prompt.

model initialization [2]. Tab. VI(c) shows a noticeable performance decline.

Prompting architecture design. We study different designs: AdaLN, Cross-attention, and ControlNet as discussed in Sec. III-B. Tab. VI(d,e,f) reveals that ControlNet performs best but still falls short of our method.

Training data and edge-aware depth loss. We initially incorporate ARKitScenes data, which only enhances performance on ARKitScenes (Tab. VI(g)). Then we add ScanNet++, which improves results on both ARKitScenes and ScanNet++ (Tab. VI(h)). However, the depth visualization remains less than ideal (Fig. 3). Tab. VI(i) show that direct supervision with pseudo GT depth from reconstruction methods decreases performance. Ultimately, employing the edge-aware depth loss that utilizes pseudo GT depth and FARO annotated GT achieves comparable performance with Tab. VI(h) but with superior thin structure depth performance as shown in Fig. 3.

Prompting strategies. In this work, we propose two prompting strategies tailored for depth upsampling and completion tasks, respectively. To assess their effectiveness, we conduct experiments on the HyperSim test set, evaluating both models under upsampling and completion scenarios. As shown in Tab. VII, each prompting strategy performs best in its designated setting. The pattern-agnostic prompting achieves comparable results in both tasks, while the upsampling prompting excels specifically in upsampling. These results indicate that both strategies are necessary: the upsampling prompting is optimal for upsampling, whereas the pattern-agnostic prompting offers broader applicability across different tasks.

Replacing the foundation model. Since our model is a general design for DPT, it can be easily adapted to other depth foundation models that also utilize the DPT structure, such as Depth Pro [9]. Our experiments demonstrate that it significantly enhances the performance of Depth Pro, as shown in Tabs. II and VI-(k), although it does not outperform our choice of Depth Anything.

Running time analysis. Our upsampling model with ViT-L runs at 20.4 FPS for an image resolution of 768×1024 on a A100 GPU. As ARKit6 supports 4K image recording, we test our model at a resolution of 2160×3840 and achieve 2.0 FPS. Note that our model can also be implemented with ViT-S, where the corresponding speeds are 80.0 and 10.3 FPS. More testing results can be found in the supp. Our completion model with ViT-L achieves a runtime of 18.2 FPS at a resolution of 768×1024 . This is slightly slower than the upsampling model, as the prompting attention block introduces additional

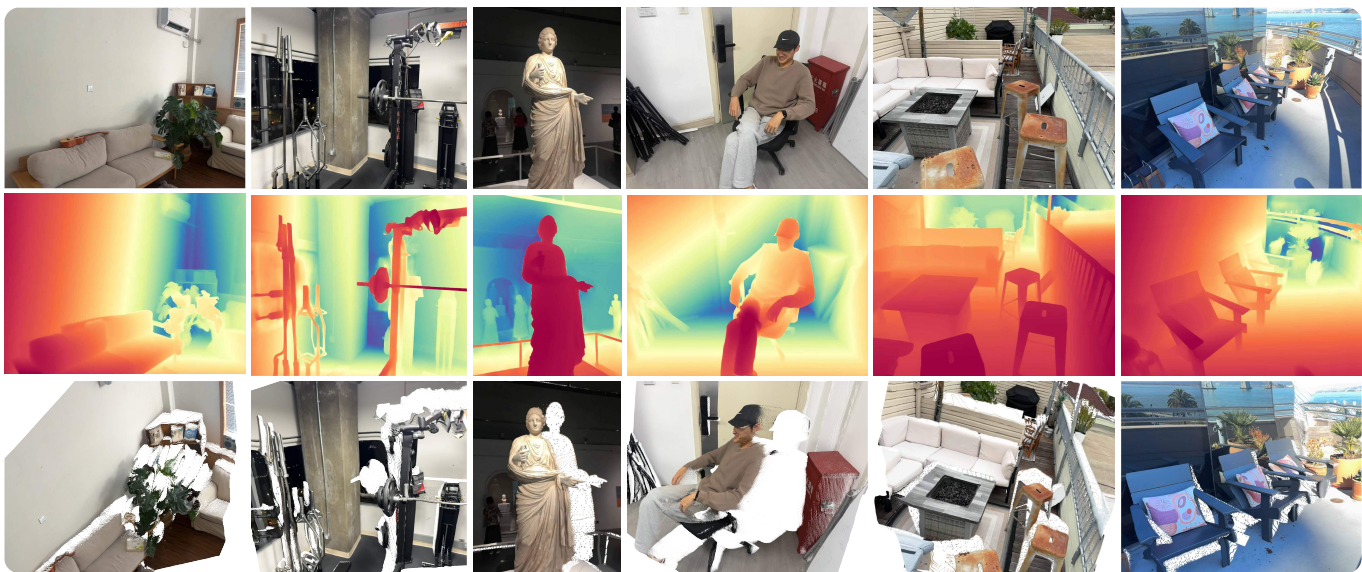


Fig. 10. Zero-shot testing on diverse scenes.

computational overhead, accounting for approximately 12% of the total computation of the depth foundation model.

D. Zero-shot Testing on Diverse Scenes

Although our model is trained on indoor scenes, it generalizes well to various scenarios, including new rooms, gyms with thin structures, poorly lit museums, human and outdoor environments, as shown in Fig. 10, highlighting the effectiveness of prompting a depth foundation model.

E. Application: Street Reconstruction

Our consistent and scale-accurate depth estimation benefits the indoor, object-level 3D reconstruction as shown in Tab. I and Figs. 5 and 8. Besides, the prompt of our model can be easily replaced with vehicle LiDAR, which enables our model to achieve large-scale outdoor scene reconstruction as shown in Fig. 9. We detail the setup in the supp.

F. Application: Generalized Robotic Grasping

We set up a robotic platform to test our model in generalized robotic manipulation (Fig. 11), which typically requires depth or RGB as observations. Good depth estimation enhances the generalization ability because it accurately describes the 3D information of surroundings [101], [102]. Specifically, we train an ACT policy [103] to grasp various objects into the box, using different types of input signals such as RGB, LiDAR, and depth data from our model. We empirically find that our model generalizes well to unseen objects like transparent and specular objects when trained on diffusive objects, outperforming RGB and LiDAR inputs as shown in Tab. VIII. This is because RGB is dominated by color, which leads to poor generalization across objects, and the iPhone LiDAR depth is noisy and lacks the capability to perceive transparent objects. Please refer to the supp. for detailed setup descriptions and videos.

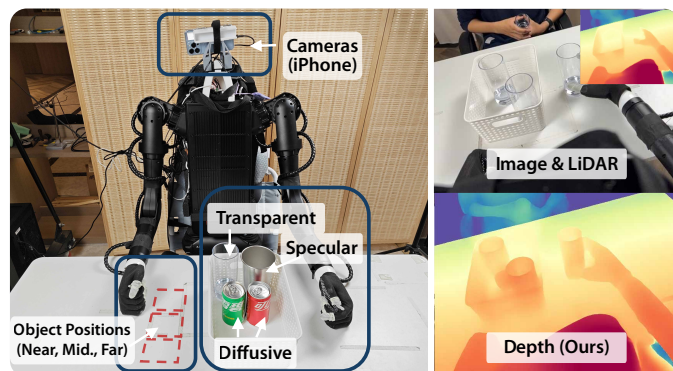


Fig. 11. Robotic grasping setup and input signal types. Our goal is to grasp objects of various types using image/LiDAR/depth inputs. Red rectangles indicate potential object positions.

TABLE VIII
GRASPING SUCCESS RATE ON VARIOUS OBJECTS. THREE NUMBERS INDICATE OBJECTS PLACED AT NEAR, MIDDLE, AND FAR POSITIONS. THE GRASPING POLICY IS TRAINED ON DIFFUSIVE AND TESTED ON ALL OBJECTS.

Input Signal	Diffusive		Transparent	Specular
	Red Can	Green Can		
Ours	1.0/1.0/1.0	1.0/1.0/1.0	0.3/1.0/1.0	0.8/1.0/0.9
LiDAR	1.0/1.0/1.0	1.0/1.0/0.2	0.5/0.4/0.0	0.7/1.0/0.0
RGB	1.0/1.0/0.0	1.0/1.0/0.0	0.2/1.0/0.0	0.0/0.9/0.9

V. CONCLUSION AND DISCUSSIONS

This paper introduced a new paradigm for metric depth estimation, formulated as prompting a depth foundation model with metric information. We validated the feasibility of the paradigm by choosing the low-cost LiDAR depth as the prompt. A scalable data pipeline was proposed to generate synthetic LiDAR depth and pseudo GT depth for training. Extensive experiments demonstrate the superiority of our method against existing monocular depth estimation and depth

completion/upsampling methods. Furthermore, we showed that it benefits for downstream tasks including 3D reconstruction and generalized robotic grasping.

Limitations and future work. This work has some known limitations. For instance, when using the iPhone LiDAR as the prompt, it cannot handle long-range depth, as the iPhone LiDAR detects very noisy depth for far objects. Additionally, we observed some temporal flickering of LiDAR depth, leading to a flickering depth prediction. These issues can be addressed in future works by considering more advanced prompt learning techniques that can extend the effective range and temporal prompt tuning.

REFERENCES

- [1] L. Yang, B. Kang, Z. Huang, X. Xu, J. Feng, and H. Zhao, “Depth anything: Unleashing the power of large-scale unlabeled data,” in *CVPR*, 2024, pp. 10371–10381.
- [2] L. Yang, B. Kang, Z. Huang, Z. Zhao, X. Xu, J. Feng, and H. Zhao, “Depth anything v2,” 2024.
- [3] B. Ke, A. Obukhov, S. Huang, N. Metzger, R. C. Daudt, and K. Schindler, “Repurposing diffusion-based image generators for monocular depth estimation,” in *CVPR*, 2024, pp. 9492–9502.
- [4] X. Fu, W. Yin, M. Hu, K. Wang, Y. Ma, P. Tan, S. Shen, D. Lin, and X. Long, “Geowizard: Unleashing the diffusion priors for 3d geometry estimation from a single image,” in *ECCV*. Springer, 2025, pp. 241–258.
- [5] S. F. Bhat, R. Birkl, D. Wofk, P. Wonka, and M. Müller, “Zoedepth: Zero-shot transfer by combining relative and metric depth,” *arXiv*, 2023.
- [6] V. Guizilini, I. Vasiljevic, D. Chen, R. Amrúş, and A. Gaidon, “Towards zero-shot scale-aware monocular depth estimation,” in *ICCV*, 2023, pp. 9233–9243.
- [7] L. Piccinelli, Y.-H. Yang, C. Sakaridis, M. Segu, S. Li, L. Van Gool, and F. Yu, “UniDepth: Universal monocular metric depth estimation,” in *CVPR*, 2024.
- [8] W. Yin, C. Zhang, H. Chen, Z. Cai, G. Yu, K. Wang, X. Chen, and C. Shen, “Metric3d: Towards zero-shot metric 3d prediction from a single image,” in *CVPR*, 2023, pp. 9043–9053.
- [9] A. Bochkovskii, A. Delaunoy, H. Germain, M. Santos, Y. Zhou, S. R. Richter, and V. Koltun, “Depth pro: Sharp monocular metric depth in less than a second,” *arXiv*, 2024.
- [10] M. Hu, W. Yin, C. Zhang, Z. Cai, X. Long, H. Chen, K. Wang, G. Yu, C. Shen, and S. Shen, “Metric3d v2: A versatile monocular geometric foundation model for zero-shot metric depth and surface normal estimation,” *TPAMI*, 2024.
- [11] T. B. Brown, “Language models are few-shot learners,” *arXiv*, 2020.
- [12] J. Achiam, S. Adler, S. Agarwal, L. Ahmad, I. Akkaya, F. L. Aleman, D. Almeida, J. Altenschmidt, S. Altman, S. Anadkat *et al.*, “Gpt-4 technical report,” *arXiv*, 2023.
- [13] R. Rombach, A. Blattmann, D. Lorenz, P. Esser, and B. Ommer, “High-resolution image synthesis with latent diffusion models,” in *CVPR*, 2022, pp. 2446–2454.
- [14] H. Liu, C. Li, Q. Wu, and Y. J. Lee, “Visual instruction tuning,” in *NeurIPS*, 2023.
- [15] H. Liu, C. Li, Y. Li, and Y. J. Lee, “Improved baselines with visual instruction tuning,” 2023.
- [16] R. Ranftl, A. Bochkovskiy, and V. Koltun, “Vision transformers for dense prediction,” in *ICCV*, 2021, pp. 12179–12188.
- [17] M. Roberts, J. Ramapuram, A. Ranjan, A. Kumar, M. A. Bautista, N. Paczan, R. Webb, and J. M. Susskind, “Hypersim: A photorealistic synthetic dataset for holistic indoor scene understanding,” in *ICCV*, 2021.
- [18] C. Yeshwanth, Y.-C. Liu, M. Nießner, and A. Dai, “Scannet++: A high-fidelity dataset of 3d indoor scenes,” in *ICCV*, 2023, pp. 12–22.
- [19] J. T. Barron, B. Mildenhall, D. Verbin, P. P. Srinivasan, and P. Hedman, “Zip-nerf: Anti-aliased grid-based neural radiance fields,” in *ICCV*, 2023, pp. 19697–19705.
- [20] G. Baruch, Z. Chen, A. Dehghan, T. Dimry, Y. Feigin, P. Fu, T. Gebauer, B. Joffe, D. Kurz, A. Schwartz *et al.*, “Arkitscenes: A diverse real-world dataset for 3d indoor scene understanding using mobile rgb-d data,” *NeurIPS*, 2021.
- [21] P. Sun, H. Kretschmar, X. Dotiwalla, A. Chouard, V. Patnaik, P. Tsui, J. Guo, Y. Zhou, Y. Chai, B. Caine *et al.*, “Scalability in perception for autonomous driving: Waymo open dataset,” in *CVPR*, 2020, pp. 2446–2454.
- [22] H. Lin, S. Peng, J. Chen, S. Peng, J. Sun, M. Liu, H. Bao, J. Feng, X. Zhou, and B. Kang, “Prompting depth anything for 4k resolution accurate metric depth estimation,” in *Proceedings of the Computer Vision and Pattern Recognition Conference*, 2025, pp. 17070–17080.
- [23] N. Silberman, D. Hoiem, P. Kohli, and R. Fergus, “Indoor segmentation and support inference from rgb-d images,” in *ECCV*. Springer, 2012, pp. 746–760.
- [24] A. Dai, A. X. Chang, M. Savva, M. Halber, T. Funkhouser, and M. Nießner, “Scannet: Richly-annotated 3d reconstructions of indoor scenes,” in *Proceedings of the IEEE conference on computer vision and pattern recognition*, 2017, pp. 5828–5839.
- [25] I. Vasiljevic, N. Kolkin, S. Zhang, R. Luo, H. Wang, F. Z. Dai, A. F. Daniele, M. Mostajabi, S. Basart, M. R. Walter, and G. Shakhnarovich, “DIODE: A Dense Indoor and Outdoor DEPTH Dataset,” *CoRR*, vol. abs/1908.00463, 2019. [Online]. Available: <http://arxiv.org/abs/1908.00463>
- [26] T. Schops, T. Sattler, and M. Pollefeys, “Bad slam: Bundle adjusted direct rgb-d slam,” in *Proceedings of the IEEE/CVF Conference on Computer Vision and Pattern Recognition*, 2019, pp. 134–144.
- [27] A. Geiger, P. Lenz, and R. Urtasun, “Are we ready for autonomous driving? the kitti vision benchmark suite,” in *Conference on Computer Vision and Pattern Recognition (CVPR)*, 2012.
- [28] J. Tang, F.-P. Tian, B. An, J. Li, and P. Tan, “Bilateral propagation network for depth completion,” *CVPR*, 2024.
- [29] M. Viola, K. Qu, N. Metzger, B. Ke, A. Becker, K. Schindler, and A. Obukhov, “Marigold-dc: Zero-shot monocular depth completion with guided diffusion,” 2024.
- [30] Y. Zuo, W. Yang, Z. Ma, and J. Deng, “Omni-dc: Highly robust depth completion with multiresolution depth integration,” *arXiv preprint arXiv:2411.19278*, 2024.
- [31] Z. Wang, S. Chen, L. Yang, J. Wang, Z. Zhang, H. Zhao, and Z. Zhao, “Depth anything with any prior,” 2025. [Online]. Available: <https://arxiv.org/abs/2505.10565>
- [32] H. Guo, H. Zhu, S. Peng, H. Lin, Y. Yan, T. Xie, W. Wang, X. Zhou, and H. Bao, “Multi-view reconstruction via sfm-guided monocular depth estimation,” in *CVPR*, 2025.
- [33] G. Xu, X. Wang, X. Ding, and X. Yang, “Iterative geometry encoding volume for stereo matching,” in *CVPR*, 2023.
- [34] A. Saxena, M. Sun, and A. Y. Ng, “Make3d: Learning 3d scene structure from a single still image,” *TPAMI*, vol. 31, no. 5, pp. 824–840, 2008.
- [35] D. Hoiem, A. A. Efros, and M. Hebert, “Recovering surface layout from an image,” *IJCV*, vol. 75, pp. 151–172, 2007.
- [36] D. Eigen, C. Puhrsch, and R. Fergus, “Depth map prediction from a single image using a multi-scale deep network,” *NeurIPS*, vol. 27, 2014.
- [37] D. Eigen and R. Fergus, “Predicting depth, surface normals and semantic labels with a common multi-scale convolutional architecture,” in *ICCV*, 2015, pp. 2650–2658.
- [38] Z. Li and N. Snavely, “MegaDepth: Learning single-view depth prediction from internet photos,” in *CVPR*, 2018.
- [39] Y. Yao, Z. Luo, S. Li, J. Zhang, Y. Ren, L. Zhou, T. Fang, and L. Quan, “Blendedmvs: A large-scale dataset for generalized multi-view stereo networks,” in *CVPR*, 2020.
- [40] J. Cho, D. Min, Y. Kim, and K. Sohn, “Diml/cvl rgb-d dataset: 2m rgb-d images of natural indoor and outdoor scenes,” *arXiv*, 2021.
- [41] K. Xian, J. Zhang, O. Wang, L. Mai, Z. Lin, and Z. Cao, “Structure-guided ranking loss for single image depth prediction,” in *CVPR*, 2020.
- [42] W. Wang, D. Zhu, X. Wang, Y. Hu, Y. Qiu, C. Wang, Y. Hu, A. Kapoor, and S. Scherer, “Tartanair: A dataset to push the limits of visual slam,” in *IROS*, 2020.
- [43] Q. Wang, S. Zheng, Q. Yan, F. Deng, K. Zhao, and X. Chu, “Irs: A large naturalistic indoor robotics stereo dataset to train deep models for disparity and surface normal estimation,” in *ICME*, 2021.
- [44] C. Wang, S. Lucey, F. Perazzi, and O. Wang, “Web stereo video supervision for depth prediction from dynamic scenes,” in *3DV*, 2019.
- [45] K. Xian, C. Shen, Z. Cao, H. Lu, Y. Xiao, R. Li, and Z. Luo, “Monocular relative depth perception with web stereo data supervision,” in *CVPR*, 2018.
- [46] R. Ranftl, K. Lasinger, D. Hafner, K. Schindler, and V. Koltun, “Towards robust monocular depth estimation: Mixing datasets for zero-shot cross-dataset transfer,” *TPAMI*, 2020.
- [47] J. He, H. Li, W. Yin, Y. Liang, L. Li, K. Zhou, H. Liu, B. Liu, and Y.-C. Chen, “Lotus: Diffusion-based visual foundation model for high-quality dense prediction,” *arXiv*, 2024.

- [48] J. He, H. Li, M. Sheng, and Y.-C. Chen, "Lotus-2: Advancing geometric dense prediction with powerful image generative model," *arXiv*, 2025.
- [49] G. Xu, H. Lin, H. Luo, X. Wang, J. Yao, L. Zhu, Y. Pu, C. Chi, H. Sun, B. Wang, G. Chen, H. Ye, S. Peng, and X. Yang, "Pixel-perfect depth with semantics-prompted diffusion transformers," in *NeurIPS*, 2025.
- [50] G. Xu, H. Lin, H. Luo, H. Sun, B. Wang, G. Chen, S. Peng, H. Ye, and X. Yang, "Pixel-perfect visual geometry estimation," *arXiv*, 2026.
- [51] H. Fu, M. Gong, C. Wang, K. Batmanghelich, and D. Tao, "Deep ordinal regression network for monocular depth estimation," in *CVPR*, 2018.
- [52] S. F. Bhat, I. Alhashim, and P. Wonka, "AdaBins: Depth estimation using adaptive bins," in *CVPR*, 2021.
- [53] —, "LocalBins: Improving depth estimation by learning local distributions," in *ECCV*, 2022.
- [54] Z. Li, X. Wang, X. Liu, and J. Jiang, "BinsFormer: Revisiting adaptive bins for monocular depth estimation," *TIP*, vol. 33, pp. 3964–3976, 2024.
- [55] Z. Li, S. F. Bhat, and P. Wonka, "Patchfusion: An end-to-end tile-based framework for high-resolution monocular metric depth estimation," 2024.
- [56] —, "Patchrefiner: Leveraging synthetic data for real-domain high-resolution monocular metric depth estimation," 2024.
- [57] W. Yin, J. Zhang, O. Wang, S. Niklaus, L. Mai, S. Chen, and C. Shen, "Learning to recover 3d scene shape from a single image," in *CVPR*, 2021, pp. 204–213.
- [58] H. Lin, S. Chen, J. Liew, D. Y. Chen, Z. Li, G. Shi, J. Feng, and B. Kang, "Depth anything 3: Recovering the visual space from any views," *arXiv*, 2025.
- [59] H. Yu, H. Lin, J. Wang, J. Li, Y. Wang, X. Zhang, Y. Wang, X. Zhou, R. Hu, and S. Peng, "Infinidepth: Arbitrary-resolution and fine-grained depth estimation with neural implicit fields," *arXiv*, 2026.
- [60] L. Mescheder, W. Dong, S. Li, X. Bai, M. Santos, P. Hu, B. Lecouat, M. Zhen, A. Delaunoy, T. Fang, Y. Tsin, S. R. Richter, and V. Koltun, "Sharp monocular view synthesis in less than a second," *arXiv*, 2025.
- [61] L. Zhang, A. Rao, and M. Agrawala, "Adding conditional control to text-to-image diffusion models," in *ICCV*, 2023, pp. 3836–3847.
- [62] G. Xu, J. Cheng, P. Guo, and X. Yang, "Attention concatenation volume for accurate and efficient stereo matching. in 2022 ieee," in *CVPR*, 2022.
- [63] G. Xu, Y. Wang, J. Cheng, J. Tang, and X. Yang, "Accurate and efficient stereo matching via attention concatenation volume," *TPAMI*, 2023.
- [64] G. Xu, X. Wang, Z. Zhang, J. Cheng, C. Liao, and X. Yang, "Ige++: iterative multi-range geometry encoding volumes for stereo matching," *arXiv*, 2024.
- [65] G. Xu, W. Yin, J. Zhang, O. Wang, S. Niklaus, S. Chen, and J.-W. Bian, "Towards domain-agnostic depth completion," *Machine Intelligence Research*, pp. 1–18, 2024.
- [66] J. Cheng, L. Liu, G. Xu, X. Wang, Z. Zhang, Y. Deng, J. Zang, Y. Chen, Z. Cai, and X. Yang, "Monster: Marry monodepth to stereo unleashes power," *CVPR*, 2025.
- [67] K. He, J. Sun, and X. Tang, "Guided image filtering," *TPAMI*, vol. 35, no. 6, pp. 1397–1409, 2012.
- [68] B. Huhle, T. Schairer, P. Jenke, and W. Straßer, "Fusion of range and color images for denoising and resolution enhancement with a non-local filter," *Computer vision and image understanding*, vol. 114, no. 12, pp. 1336–1345, 2010.
- [69] J. Kopf, M. F. Cohen, D. Lischinski, and M. Uyttendaele, "Joint bilateral upsampling," vol. 26, no. 3, pp. 96–es, 2007.
- [70] D. Ferstl, C. Reinbacher, R. Ranftl, M. R  ther, and H. Bischof, "Image guided depth upsampling using anisotropic total generalized variation," 2013, pp. 993–1000.
- [71] J. Yang, X. Ye, K. Li, C. Hou, and Y. Wang, "Color-guided depth recovery from rgb-d data using an adaptive autoregressive model," vol. 23, no. 8, pp. 3443–3458, 2014.
- [72] Y. Zhang, X. Guo, M. Poggi, Z. Zhu, G. Huang, and S. Mattocchia, "Completionformer: Depth completion with convolutions and vision transformers," 2023, pp. 18 527–18 536.
- [73] X. Cheng, P. Wang, C. Guan, and R. Yang, "Cspn++: Learning context and resource aware convolutional spatial propagation networks for depth completion," vol. 34, no. 07, 2020, pp. 10 615–10 622.
- [74] X. Cheng, P. Wang, and R. Yang, "Learning depth with convolutional spatial propagation network," vol. 42, no. 10, pp. 2361–2379, 2019.
- [75] J. Tang, F.-P. Tian, W. Feng, J. Li, and P. Tan, "Learning guided convolutional network for depth completion," vol. 30, pp. 1116–1129, 2020.
- [76] X. Liu, X. Shao, B. Wang, Y. Li, and S. Wang, "Graphcspn: Geometry-aware depth completion via dynamic gcns." Springer, 2022, pp. 90–107.
- [77] Z. Sun, W. Ye, J. Xiong, G. Choe, J. Wang, S. Su, and R. Ranjan, "Consistent direct time-of-flight video depth super-resolution," in *CVPR*, 2023, pp. 5075–5085.
- [78] Y. Lin, T. Cheng, Q. Zhong, W. Zhou, and H. Yang, "Dynamic spatial propagation network for depth completion," in *AAAI*, vol. 36, no. 2, 2022, pp. 1638–1646.
- [79] A. Conti, M. Poggi, V. Cambareri, and S. Mattocchia, "Depth on demand: Streaming dense depth from a low frame rate active sensor," *arXiv*, 2024.
- [80] B. Tan, C. Sun, X. Qin, H. Adai, Z. Fu, T. Zhou, H. Zhang, Y. Xu, X. Zhu, Y. Shen, and N. Xue, "Masked depth modeling for spatial perception," *arXiv*, 2026.
- [81] Y. Li, X. Liu, W. Dong, H. Zhou, H. Bao, G. Zhang, Y. Zhang, and Z. Cui, "Deltar: Depth estimation from a light-weight tof sensor and rgb image," in *ECCV*. Springer, 2022, pp. 619–636.
- [82] X. Ren, W. Wang, D. Cai, T. Tuominen, J. Kannala, and E. Rahtu, "Mushroom: Multi-sensor hybrid room dataset for joint 3d reconstruction and novel view synthesis," in *WACV*, 2024, pp. 4508–4517.
- [83] J.-H. Park, C. Jeong, J. Lee, and H.-G. Jeon, "Depth prompting for sensor-agnostic depth estimation," in *CVPR*, 2024, pp. 9859–9869.
- [84] A. Kirillov, E. Mintun, N. Ravi, H. Mao, C. Rolland, L. Gustafson, T. Xiao, S. Whitehead, A. C. Berg, W.-Y. Lo *et al.*, "Segment anything," in *ICCV*, 2023, pp. 4015–4026.
- [85] R. Birkel, D. Wofk, and M. M  ller, "Midas v3. 1—a model zoo for robust monocular relative depth estimation," *arXiv*, 2023.
- [86] R. Rombach, A. Blattmann, D. Lorenz, P. Esser, and B. Ommer, "High-resolution image synthesis with latent diffusion models," in *CVPR*, 2022, pp. 10 684–10 695.
- [87] W. Peebles and S. Xie, "Scalable diffusion models with transformers," in *ICCV*, 2023, pp. 4195–4205.
- [88] T. Karras, S. Laine, and T. Aila, "A style-based generator architecture for generative adversarial networks," in *CVPR*, 2019, pp. 4401–4410.
- [89] E. Perez, F. Strub, H. De Vries, V. Dumoulin, and A. Courville, "Film: Visual reasoning with a general conditioning layer," in *AAAI*, vol. 32, no. 1, 2018.
- [90] A. Vaswani, "Attention is all you need," *Advances in Neural Information Processing Systems*, 2017.
- [91] T. Xie, X. Chen, Z. Xu, Y. Xie, Y. Jin, Y. Shen, S. Peng, H. Bao, and X. Zhou, "Envgs: Modeling view-dependent appearance with environment gaussian," *CVPR*, 2025.
- [92] Y. Yan, H. Lin, C. Zhou, W. Wang, H. Sun, K. Zhan, X. Lang, X. Zhou, and S. Peng, "Street gaussians for modeling dynamic urban scenes," *ECCV*, 2024.
- [93] B. Mildenhall, P. P. Srinivasan, M. Tancik, J. T. Barron, R. Ramamoorthi, and R. Ng, "Nerf: Representing scenes as neural radiance fields for view synthesis," *ECCV*, vol. 65, no. 1, pp. 99–106, 2020.
- [94] Y. Cabon, N. Murray, and M. Humenberger, "Virtual kitti 2," 2020.
- [95] J. L. G  mez, M. Silva, A. Seoane, A. Borr  s, M. Noriega, G. Ros, J. A. Iglesias-Guiti  n, and A. M. L  pez, "All for one, and one for all: Urbansyn dataset, the third musketeer of synthetic driving scenes," *Neurocomputing*, vol. 637, p. 130038, 2025.
- [96] N. Karaev, I. Rocco, B. Graham, N. Neverova, A. Vedaldi, and C. Rupprecht, "Dynamicstereo: Consistent dynamic depth from stereo videos," *CVPR*, 2023.
- [97] C. Xian, K. Qian, Z. Zhang, and C. C. Wang, "Multi-scale progressive fusion learning for depth map super-resolution," *arXiv*, 2020.
- [98] R. Jensen, A. Dahl, G. Vogiatzis, E. Tola, and H. Aan  s, "Large scale multi-view stereopsis evaluation," in *CVPR*, 2014, pp. 406–413.
- [99] J. Straub, T. Whelan, L. Ma, Y. Chen, E. Wijmans, S. Green, J. J. Engel, R. Mur-Artal, C. Ren, S. Verma *et al.*, "The replica dataset: A digital replica of indoor spaces," *arXiv*, 2019.
- [100] X. He, J. Sun, Y. Wang, S. Peng, Q. Huang, H. Bao, and X. Zhou, "Detector-free structure from motion," *CVPR*, 2024.
- [101] Y. Ze, Z. Chen, W. Wang, T. Chen, X. He, Y. Yuan, X. B. Peng, and J. Wu, "Generalizable humanoid manipulation with improved 3d diffusion policies," *arXiv*, 2024.
- [102] P. Hua, M. Liu, A. Macaluso, Y. Lin, W. Zhang, H. Xu, and L. Wang, "Gensim2: Scaling robot data generation with multi-modal and reasoning llms," *arXiv*, 2024.
- [103] T. Z. Zhao, V. Kumar, S. Levine, and C. Finn, "Learning fine-grained bimanual manipulation with low-cost hardware," *Robotics: Science and Systems*, 2023.